Applied Physics A (2024) 130:343
https://doi.org/10.1007/s00339-024-07468-w

Applied Physics A
Materials Science & Processing

Diffuse to normal ferroelectric transition in Gd-substituted BBTO Aurivillius ceramics

Tirupathi Patri[1] · K. S. K. R. Chandra Sekhar[2] · Ammar Mohamed Tighezza[3] · Deepash Shekhar Saini[4] · P. Rosaiah[5] · Avijit Ghosh[6]

Received: 6 December 2023 / Accepted: 21 March 2024 / Published online: 26 April 2024

Abstract

A comprehensive investigation of the structural, microstructural, ferroelectric, and dielectric relaxation characteristics was accomplished on Gd-substituted barium bismuth titanate ($BaBi_4Ti_4O_{15}$) (BBTO) Aurivillius ceramics. The Rietveld refined X-ray diffraction confirmed that the low-concentration (≤ 0.10) of Gd ions as a more stable orthorhombic with $A2_1am$ phase and to higher concentration (> 0.10) as dual phase orthorhombic "$A2_1am + F2mm$" space group. The inherent plate-like grain morphology was characterized by a scanning electron microscope. A discernible microstructural phonon modification in Raman spectroscopy analysis exposed changes with temperature variations confirms of dual-phase pattern at increased dopant concentrations. T-dependent dielectric study reveals a shifting Curies Weiss (T_m) transition towards lower temperature was noticed with an increase of Gd dopant. The relaxor ferroelectric phase transitions were detected using the modified Curie–Weiss law such as Vogel–Fulcher (VF), Cluster Glass (CG), and Stretched string (SS) models. The VF fitting was more stabilized for lower concentrations (Gd; $x \leq 0.10$). Furthermore, the CG model was appropriate for the higher concentration of dopant (Gd; $x > 0.10$) indicating the stabilization of the relaxor ferroelectric nature. The temperature-dependent dielectric studies reveal a normal ferroelectric to relaxor ferroelectric crossover of 0.20 implying a reduction in interaction within the polar regions. The observed relaxor-like dielectric behavior suggests the generation of small-sized polar regions due to an imbalance of charge in compensation of the Bi_2O_2 layer for higher dopant concentrations. The randomly weak interaction between the small polar regions leads to a critically slowed down of polar regions dynamics below. The soft ferroelectric P-E loops with weak loop character of well predominant shape were observed in Gd-substitution BBTO ceramics.

Keywords Aurivillius ceramics · Orthorhombic crystal system · Vogel–Fulcher relation · Relaxor ferroelectrics

✉ Tirupathi Patri
ptirupathi36@gmail.com

✉ Avijit Ghosh
avijitphy@gmail.com

[1] Department of Physics, Rajiv Gandhi University of Knowledge Technologies, Srikakulam, Andhra Pradesh 532402, India

[2] Department of Physics, V. R. Siddhartha Engineering College, Vijayawada, Andhra Pradesh 520007, India

[3] Department of Chemistry, College of Science, King Saud University, P. O. Box 2455, 11451 Riyadh, Saudi Arabia

[4] Department of Physics, Deen Dayal Upadhaya Gorakhpur University, Gorakhpur, Utter Pradesh 273009, India

[5] School of Mechanical Engineering, Yeungnam University, 280 Daehak-Ro, Gyoungsan-Si, Gyeongsangbuk-Do 38541, Republic of Korea

[6] Departments of Physics, Central University of Jharkhand, Ranchi, Jharkhand 835205, India

1 Introduction

The well-known lead-based piezoelectric and ferroelectric perovskite materials i.e., $PbTiO_3$, $Pb(Mg_{1/3}Nb_{2/3})O_3$, $(Pb_{1-x}La_{2x/3})(Zr_{1-y}Ti_y)O_3$, etc. have trigged many challenges with poor fatigue resistance, and low Curie temperature, which limits for practical electronic applications near at room temperature (RT) [1–4]. Meanwhile, in the high-temperature regime, these perovskite materials have practical application limitations. Furthermore, the toxic nature of lead has great environmental issues [3, 4]. Therefore, a new search has been initiated for alternative high Curie (T_C) temperature and environmentally friendly piezoelectric materials. Among the reports, the bismuth-based Aurivillius perovskite ferroelectric family has shown desirable relaxor properties, high piezoelectric coefficient, good polarization fatigue resistance, and high T_C temperatures [5–7].

The general Aurivillius Bismuth layered-structured ceramics are formulated as $(A_{n-1}B_n O_{3n+1})^{2-}$ $(Bi_2O_2)^{2+}$, (ABO-BO) where *n* denotes the number of perovskite unit cell layers sandwiched between two fluorite-like $(Bi_2O_2)^{2+}$ layers. These ceramics exhibit excellent ferroelectric polarization with a large piezoelectric constant and large T_C temperature well above 400 ℃, in contrast to conventional lead-based perovskite materials [5–7]. The remarkable polarization, combined with a large piezoelectric constant, has garnered significant interest in layered ferroelectric perovskite materials for high-temperature piezoelectric devices, nonvolatile random-access memories (NVRAM), transducers, sensors, and various other applications [5–7]. Previous reports have focused on $Bi_4Ti_3O_{12}$ ($n=3$) and $Bi_5Ti_4O_{15}$ ($n=4$), bismuth-based Aurivillius phase materials, due to their wide range of multifunctional characteristics, including optical, piezoelectric, and soft relaxor ferroelectric properties, making them promising candidates for energy harvesting devices [8–11].

Subsequently, the researchers discovered a new series with modified $Bi_5Ti_4O_{15}$ ($n=4$) ceramics using different divalent substitution elements (A = Ba, Sr, Ca) at the A-site (Bi-site) leading to new series of ferroelectric materials i.e., $ABi_4Ti_4O_{15}$ (ABTO) series (A = Ba, Sr, Ca). In the $ABi_4Ti_4O_{15}$ series (ABTO) (A = Ba, Sr, Ca) a particular emphasis has been placed on $BaBi_4Ti_4O_{15}$ (BBTO) ceramics (internal structure formula of $(Bi_2O_2)^{2+}$ and $(BaBi_2Ti_4O_{13})^{2-}$ because of relaxor ferroelectricity, large polarizations, and high piezoelectric constant. This is contrast to conventional ferroelectric nature observed in $SrBi_4Ti_4O_{15}$ and $CaBi_4Ti_4O_{15}$ ceramics [11–14].

Over the past decades, a special category of Aurivillius layered ferroelectrics materials, specifically $BaBi_4Ti_4O_{15}$ (BBTO) ceramics, has garnered significant attention due to their extraordinary piezoelectric, and relaxor activity for electro-caloric and electromechanical property for piezoelectric/ electro-strictive actuator, and sensor applications. The literature report suggests, the internal crystal structure of BBTO compound is orthorhombic crystal system with $A2_1am$ space group at RT. In addition, a tetragonal phase with I4/mmm space group far above RT at the Curie temperature ($T_C = 415$ ℃) noticed that notified as ferroelectric to paraelectric phase transition [15, 16].

One of the drawbacks in BBTO Aurivillius ceramics includes the dominance of oxygen vacancies in high-temperature sintering process due to the volatilization of bismuth to maintain charge neutrality. In Bi-based Aurivillius ceramics, oxygen vacancies might be preferably present in the vicinity of Bi-ions, which could be more inertia to enhance ferroelectric character [15, 16]. These internal dominant oxygen vacancies in Bi-based Aurivillius ferroelectrics provide several vital negative effects such as fatigue ferroelectric character, pinning at domain walls, enhancing leakage current, trapping charge carriers in defect domains, screening of electric field near the space charge region and impeding the displacement of Ti^{4+} ion [16, 17]. For practical applications such as memories, low conductivity and low dielectric loss with high fatigue ferroelectric character are important, these are diminished by oxygen vacancies in BBTO ceramics. In the quest of modifying the aforementioned limitations of Aurivillius BBTO ceramics and to enhance the piezoelectric/ferroelectric, dielectric character of the ceramics, many attempts have been understand using the dopant in A and/or B-site for BBTO ceramics [18–20].

Additionally, the principal drawbacks associated with iron contained ceramics are high leakage current and low electric resistivity due to oxygen vacancies and ionic valence fluctuations. Both the grain interior and grain boundaries play a pivotal role in tuning the dielectric and electrical properties in Bi-based ceramics. Therefore, an alternative noteworthy strategy employed to suppress the leakage current and improve the electrical properties of Bi-based material is to substitution of iron at Bi-site. The valance fluctuations of the iron ion at the Bi-site might affect the ferroelectric distortion and leads to the multiferroic character of the Aurivillius ceramics. Furthermore, the substitution of 4*f* elements is also capable to suppress the leakage current and improve the electrical properties of Bi-based materials [21, 22].

Recent reports highlights, the substitution of 4*f* rare earth elements such as Sm, Pr, Nd, and La can reduce the conductive nature and reduced defect dipole on account of suppress the oxygen vacancies [21–24]. On account this, the RE-substitution in BBTO ceramics greatly affects the ferroelectric distortion of bismuth-contained compounds due to weaken the Bi–O hybridization and inducing the effect of ionic size. Consequently, recent studies have reported the advent of diffuse or relaxor dielectric characteristics in rare earth (RE) substitution BBTO compounds. In the context of the existing literature on BBTO ceramics, the partial substitution of bismuth with stable trivalent RE cations has proven to be an effective resources of reducing oxygen vacancies and improving better electrical properties [24].

The advent of relaxor behavior in Aurivillius BBTO ferroelectric ceramics is primarily attributed to the significant polarizability owing to mismatch between the $(A_{n-1}B_nO_{3n+1})^{2-}$ perovskite units and the interconnected $(Bi_2O_2)^{2+}$ layers that leads to formation of small embedded polar nanoregions [25]. Furthermore, the static structural disorder in characteristic layers and the statistical distribution of polar nanoregions across a broad temperature range. The nanoscopic heterogeneity seems to be an inherent part of the relaxor, but mechanisms of how the polar nanoregions appear and evolve upon cooling are currently pursued in research arena [25].

Till now, there is no available literature reports on Gd-substituted BBTO (BBGTO) Aurivillius ceramics. Therefore, we synthesized Gd-substituted BBTO ceramic and

examined the influence of Gd^{3+} substitution on the structural, microstructural, dielectric, and ferroelectric properties [26]. In addition, we studied the relaxor-like characteristics observed by considering different models based on the correlation length and interaction between the polar regions arising due to site selectivity of Gd dopant in BBTO ceramics. The details of room temperature ferroelectric property were described in Gd substituted BBTO ceramics to explain intrinsic relaxor activity.

2 Experimental details

The $BaBi_{4-x}Gd_xTi_4O_{15}$ (BBTO) 4-layer Aurivillius ceramic oxides (x = 0.00, 0.10, 0.20 and 0.30) were synthesized by conventional solid-state reaction method using high-purity (≥ 99.99%) Bi_2O_3, TiO_2, $BaCO_3$, and Gd_2O_3 powders. The stoichiometric amounts of powders were mixed in an agate mortar using acetone as a wet medium to obtain a homogeneous mixture. An extra 5 wt % Bi_2O_3 was added to the mixture to compensate the loss of bismuth oxides during sintering at elevated temperatures. Repeated grinding and calcination was carried out at 850 ℃, 900 ℃ for 4 h, respectively [24, 27]. The calcined powder was reground with 5% polyvinyl alcohol (PVA) binder before being pressed bilaterally into pellets. Subsequently, the pressed pellets were sintered at 1100 ℃ for 4 h to obtain dense $BaBi_{4-x}Gd_xTi_4O_{15}$ ceramics. The formation of crystallinity of the ceramics was investigated by powder X-ray diffraction technique using Cu-Kα radiation of an X-ray diffractometer (PHILIPS-PW3373 XPERT-PRO) within the angular range $20^o \le 2\theta \le 80^o$ and at a scanning rate 0.053°/sec. Consequently, Rietveld's refinement of the ceramics powder samples was carried out by FullProf software. The surface morphology of the sintered pellets was observed by using field-emission scanning electron microscopy (FE-SEM, Sirion 200, FEI Company). The Microstructure and spin-phonon mode vibration of the ceramics were investigated by Confocal micro-Raman spectrometer (Witac Alpha 300) with a wavelength of 532 nm excitation source in the wave number region from 50 to 1000 cm^{-1}. The sintered pellets were coated by silver (Ag) as electrodes for electrical measurements. The temperature dependent dielectric measurements were carried out with Wayne Kerr 6500B impedance analyzer in the temperature range of 30 to 500℃ and within frequencies of 100 Hz to 1 MHz. Room temperature Ferroelectric P-E hysteresis loop measurements were carried out for silver electroded and poled ceramic pellets using a TF-Analyzer 2000 (aixACCT systems, GmbH).

3 Results and discussion

3.1 Structural phase transitions

The room temperature XRD patterns of Gd-substituted BBTO ceramics with x = 0.00, 0.10, 0.20, and 0.30 are illustrated in Fig. 1. All observed diffraction peaks of the samples were successfully indexed to the standard diffraction patterns (ICSD—99,501) of the $BaBi_4Ti_4O_{15}$ Aurivillius phase, indicating the formation of an orthorhombic structure with $A2_1am$ space group. Remarkably, the most intense diffraction peaks (119) and (200) shifted toward higher angles with increasing dopant concentration in the Bi-site of BBTO ceramics, which reflect a change in internal structural modification. Furthermore, Rietveld refinement technique adopted broadly to analyze the structure of $BaBi_{4-x}Gd_xTi_4O_{15}$ (x = 0.00, 0.10, 0.20, and 0.30) ceramics. The pristine BBTO compound (x = 0.00) was well-fitted to the orthorhombic structure of A21am space group [24, 27].

Furthermore, the dopant of Gd in BBTO compounds, as considered at Bi-site are in identical Wyckoff positions and thermal factors, where the total occupancy for both the Bi-sites is maintained to unity. Then the lattice parameters were refined using the Rietveld refinement technique with profile fitting prior to the structural refinement of all the Gd substitution specimen. Nevertheless, the experimental patterns are in well agreement with calculated XRD pattern as reasonably based on the low values of refined reliability factors. In addition, the composition for x > 0.10 concentration, the slight large value of goodness of fitting parameter and R_p, R_{wp} are noticed.

The experimental pattern well matched with the calculated XRD pattern of Gd-substituted BBTO (x = 0.00, 0.10, 0.20, and 0.30) Aurivillius ceramics as well as confirmed

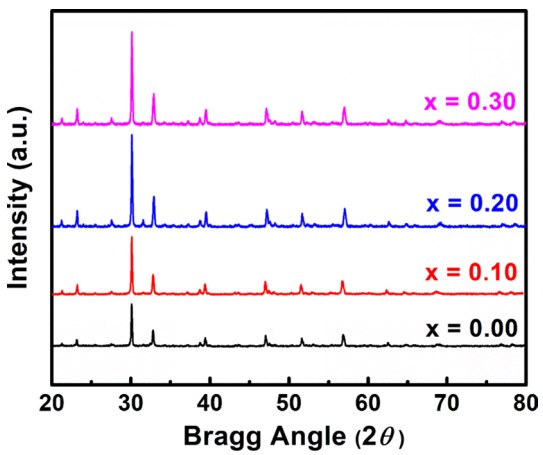

Fig. 1 Room temperature XRD patterns of $BaBi_{4-x}Gd_xTi_4O_{15}$ ceramics (x = 0.00, 0.10, 0.20, 0.30)

an orthorhombic crystal system with $A2_1am$ space group as with pristine compound of BBTO is shown in Fig. 2a–d [28, 29]. The obtained structural lattice parameters, the goodness of fitting, and orthorhombic lattice distortion (a/b) ratios are listed in Table 1. It is noticed from Table 1 with increase of ''x'', lattice parameters a and b decrease, and then the c lattice parameter also decreases. Hence, the volume (V) of the unit cell decreases with the increase of Gd-dopant in BBTO ceramics. For $x > 0.10$ concentration onward, a slight difference of a and b parameters is obtained and thus distortion

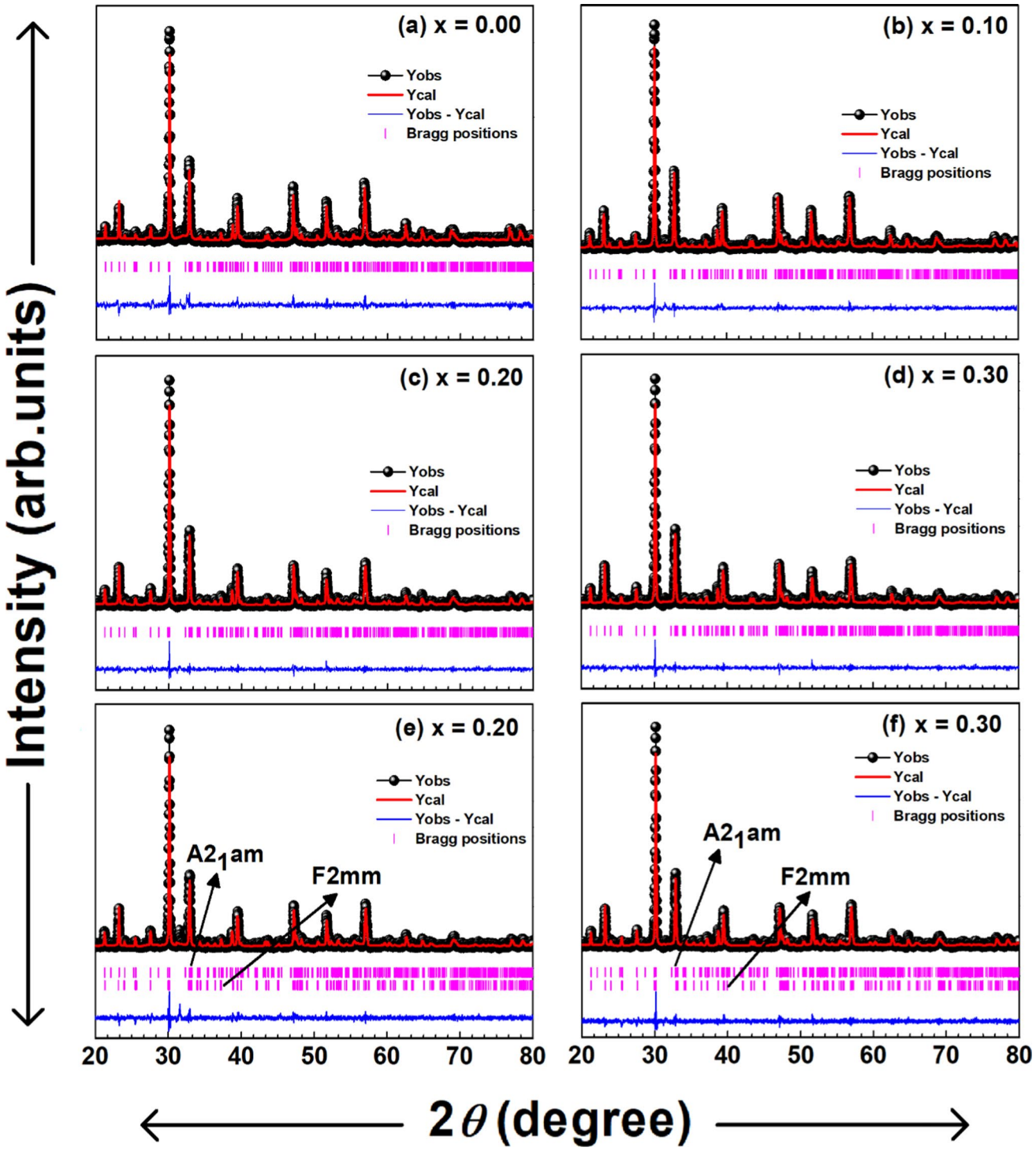

Fig. 2 **a** Rietveld refined XRD patterns of $BaBi_{4-x}Gd_xTi_4O_{15}$ indicates the presence of $A2_1am$ phase for lower concentration, while with $A2_1am + F2mm$ phases for higher concentration

Table 1 Crystallite size, Grain Size, Lattice parameters and Observed factors from Rietveld refinement for Gd-substituted BBTO ceramics

Gd concentration (x) mol%	x = 0.00	x = 0.10	x = 0.20	x = 0.30
Crystallite Size	320 nm	347 nm	370 nm	245 nm
Grain Size	3.45 µm	3.32 µm	3.89 µm	4.56 µm
Lattice Parameters (Å)	Orthorhombic ($A2_1am$)			
	a = 5.4690, b = 5.4577, and c = 41.872 V = 1249.80 Å^3	a = 5.4670, b = 5.4551, and c = 41.860 V = 1248.53 Å^3	a = 5.4470, b = 5.4348, and c = 41.8120 V = 1237.77 Å^3	a = 5.4590, b = 5.4550, and c = 41.865 V = 1246.24 Å^3
			Orthorhombic (F2mm)	
			a = 5.4572, b = 5.4506, and c = 41.6256 V = 1238.15 Å^3	a = 5.4869, b = 5.4690, and c = 40.8694 V = 1226.40 Å^3
Phase contribution (%)	$A2_1am$ (100%)	$A2_1am$ (100%)	$A2_1am$ (99.65%) + F2mm (0.35%)	$A2_1am$ (98.01%) + F2mm (1.99%)
Density (g/cm^3)	7.446	7.432	7.31	7.36
$\frac{(a-b)}{(a+b)}$	1.0016	1.0021	1.0036	0.99
Reliability Factors (%)	R_p = 7.21, R_{wp} = 9.17, and R_{exp} = 11.21	R_p = 7.24, R_{wp} = 9.91, and R_{exp} = 11.92	R_p = 7.65, R_{wp} = 8.98, and R_{exp} = 10.45	R_p = 7.84, R_{wp} = 9.19, and R_{exp} = 11.12
Bragg – R factors (%)	R_B = 9.17 and R_f = 8.38	R_B = 6.93 and R_f = 7.34	R_B = 10.01 and R_f = 13.1	R_B = 12.8 and R_f = 19.1
χ^2	3.31	2.90	5.54	5.34

(a/b) ratio is also decreased and then it converges to ≈ 1, (i.e., a = b ≠ c) as transformed towards a tetragonality phase.

Therefore, a more stable structure of orthorhombic phase for F2mm (A) space group with less distortion near to tetragonality premium was refined was not accepted with reasonable parameters. Later on, for concentration of BBGTO for x = 0.20 and 0.30 ceramics are refined with both Orthorhombic of $A2_1am$ + F2mm (A + F) phases dual phase [30]. A considerable refinement was noticed with the less goodness of fitting parameters when compared with pure phase of orthorhombic crystal system for $A2_1am$ space group. Therefore, we can confirm that the higher substitution of Gd (≥ 0.20) in BBTO Aurivillius ceramics possess the dual phase coexistence i.e., a major Orthorhombic $A2_1am$ and a minor Orthorhombic F2mm phases [30–32].

Distortion in structures arise due to effect of electronic density or/and ionic radii difference of dopant element. In Aurivillius ceramics n = 4 layered BBTO, Bi atoms occupy both coordinated sites i.e., tetrahedral coordination (Bi in $[Bi_2O_2]^{2+}$ Layers), that each Bi atom is surrounded by four oxygen atoms arranged in a tetrahedral having ionic radii 0.92 Å. On the other hand, an Octahedral Coordination (Bi in the $[BaBi_2Ti_4O_{13}]^{2-}$ Perovskite Layer), where each Bi atom is surrounded by six oxygen atoms arranged in an octahedral manner having ionic radii 1.17 Å. In general, the ionic radius of the dopant element Gd^{3+} is 0.94 Å, which is relatively large for occupying tetrahedral sites. Consequently, Gd^{3+} ions are bound to occupy octahedral sites within the Bi ion lattice. Furthermore, a large variation of ionic radius of the 4f-Gd^{3+} ion and Bi^{3+} (RBi^{3+} = 1.17 Å), and the presence of a larger number of ions at the A-site (Gd/Ba/Bi elements) of Aurivillius phase can induce a local field. Hence, a structural distortion at the octahedral sites in Gd-BBTO Aurivillius ceramics might induced. As a consequence, high dopant concentration of Gd^{3+} in BBTO results in the coexistence of a symmetric phase with an orthorhombic (F2mm) crystal system and an $A2_1am$ space group, which is consistent with the reported XRD results [31, 32].

3.2 Room temperature Phonon mode analysis

The diffuse relaxor ferroelectric properties are interlinked to the presence of nanoregions, which strongly correlate with structural defects or/and modifications in the crystals of the ceramics. The correlation of nanoregions with structural, dielectric, and ferroelectric property cannot be distinguished directly by diffraction studies, as the diffraction techniques include only reflecting spatial average effect of the materials. Therefore, an alternative technique one is Raman scattering have a shorter characteristic length scale, which probes structural properties and spin-phonon correlation in materials. Henceforth, temperature dependent Raman scattering method was adopted to study the polar nanoregions and phonon anomaly nearer to phase transitions regions. Fig. 3a depicts the RT Raman spectra of Gd-substitution BBTO Aurivillius ceramics in the wavenumber range of 55

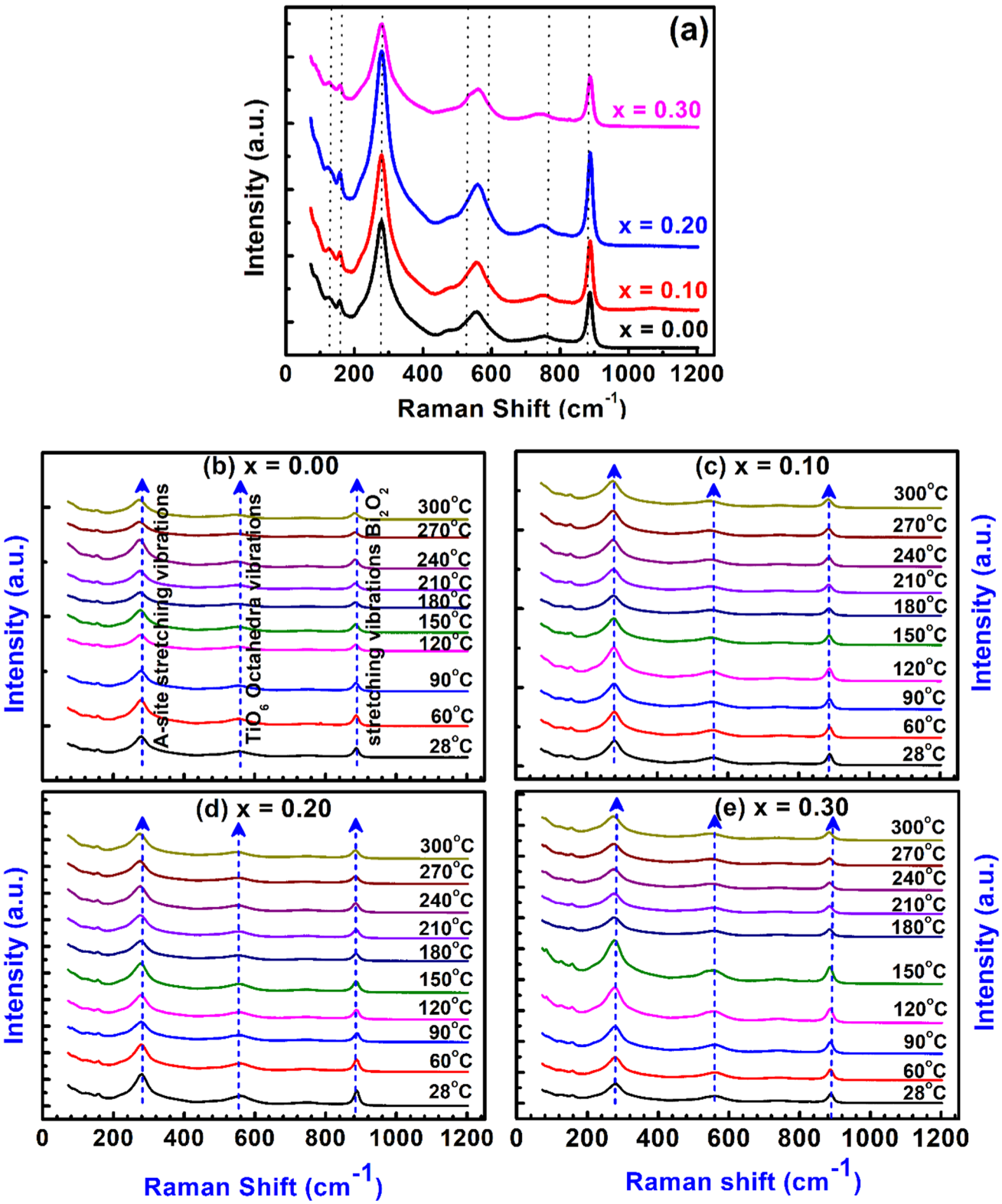

Fig. 3 Temperature dependent Raman spectra: (**a**) room temperature Raman spectral lines (**b**–**e**) Temperature dependent Raman spectral lines of $BaBi_{4-x}Gd_xTi_4O_{15}$ ceramics (x = 0.00, 0.10, 0.20, 0.30) at RT to 300 C

to 1000 cm^{-1}. The observed Raman modes at room temperature is 64, 127, 157, 278 486, 555, 753, and 887 cm^{-1} are represented with dashed-dotted lines in Fig. 3(a) are well matched with recent reports [22]. In layered Aurivillius ceramics Raman modes are categorized into three regions based on their interatomic molecular vibration frequencies i.e., (i) low frequency modes below 200 cm^{-1} and (ii) intermediate frequency range from 200 to 800 cm^{-1}, and (iii) a high frequency mode above 800 cm^{-1}. The low frequency modes below 200 cm^{-1} noticed at 64, 127 and 157 cm^{-1} are assigned to A-site relative vibration of pseudo-perovskite layer. The first one nearer to 64 cm^{-1} is assigned as a 'rigid layer' mode reflecting the Bi^{3+} ions vibration in Bi_2O_2 layers as insensitive with dopant substitution. The modes at 127 and 157 cm^{-1}, related to the vibration of the A-site ions of the pseudo perovskite blocks slightly decrease in intensity as detected. Additionally, the intermediate frequency range observed at 278 486, 555, 753 cm^{-1} corresponds to the torsional and bending of TiO_6 octahedra vibration and Ba–O modes. The Raman mode at 575 cm^{-1} slightly shift towards high wavenumber side with the substitution of Gd ion in BBTO as noticed [22]. These results reflect the blue shifts, which are more reasonably augmented for reinforcement of the binding strength in the connection of TiO_6 octahedra and Bi_2O_2 perovskite layers. Subsequently the incorporation of Gd^{3+} ion into Bi_2O_2 layers induces the bond relaxation in layers, hence the neighboring TiO_6 octahedra might shrink which results in the increase in bond energy. The high frequency mode at 887 cm^{-1} reflects the stretching mode of TiO_6 octahedra, on account of BO_6 octahedral stretching vibration in BBTO ceramics. The substitution of Gd^{3+} ion at Bi-site in BBTO Aurivillius ceramics provided a slight broaden in peak width as well increase in intensity was noticed up to x = 0.20 concentrations, then it deteriorated for higher substitutions [33].

3.3 Temperature dependent phonon mode analysis

Temperature dependent vibrational modes were presented to clearly specify the spin-phonon coupling and internal structural order with the variation of temperature. Figure 3b–e displays the temperature-dependent Raman spectra of Gd-substituted BBTO Aurivillius ceramics from the compositional range x = 0.00–0.30 respectively. From Fig. 3b–e, it reveals the presence of 8 Raman modes within the wavenumber range of 55–1000 cm^{-1}. The retraced 8 Raman modes are retained the same position of wavenumbers up to probe temperature 200 °C, and then above 200 °C, a slight shifting of Raman spectra towards the low wavenumber side was noticed. Remarkably, the most intense and significant Raman modes at 278, 555, and 887 cm^{-1}, associated with A_1-stretching vibrations, TiO_6 octahedral vibrations, and Bi_2O_2 layered stretching modifications, displayed a systematic decrease in intensity and a shift towards lower wavenumbers, as depicted in Fig. 4a–c. The changes in A-site (Bi-O) stretching vibrations and Bi_2O_2 layered stretching modifications suggest that there is most possible occupancy of Gd^{3+} ion at Bi-tetrahedral sites rather than pseudo perovskite layered sites [29, 33]. A similar behavior was noticed for all Gd-substituted BBTO ceramics as trend stated above. It indicates that the more amount of dopant element in BBTO ceramics leads towards the internal structural modifications at higher temperature regime. This study suggests that the high concentration of Gd-dopant may create

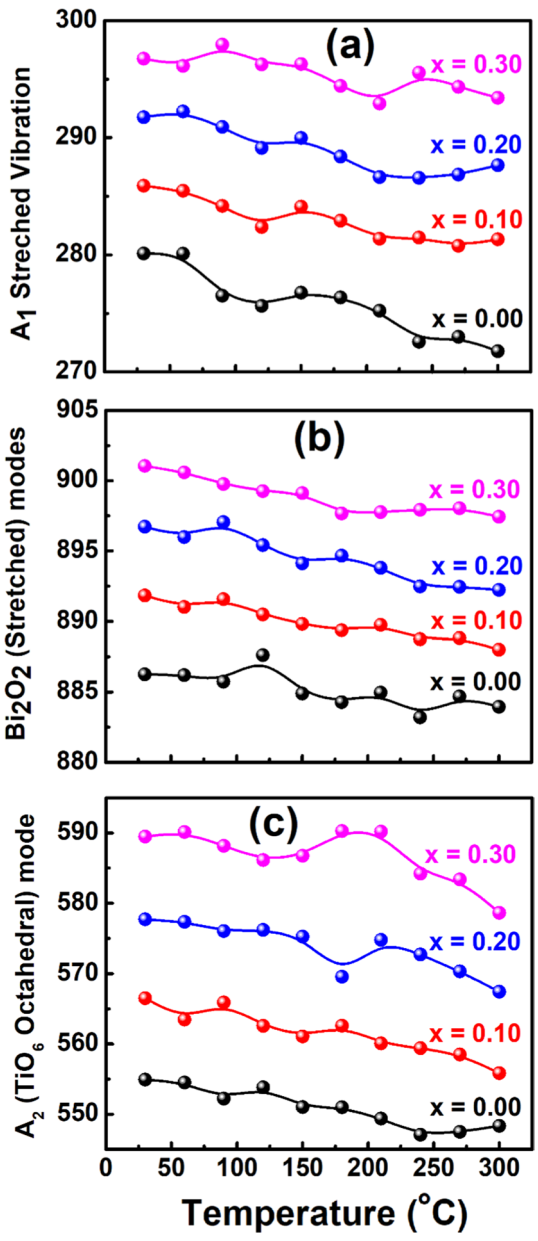

Fig. 4 T- dependent Raman spectral mode (A_1, A_2 and B_1) lines variation of dependent of $BaBi_{4-x}Gd_xTi_4O_{15}$ ceramics (x = 0.00, 0.10, 0.20, 0.30)

an internal strain both at the A-site and the layers connected to the Aurivillius samples. This disturbance arises from the relative displacement between cations and anions, which dictates local internal structural modifications and gives rise to the formation of multiple polarization fields. Consequently, these elusive alterations play a key role in inducing changes in the intrinsic physical properties.

3.4 Surface morphology studies

Figure 5a–d illustrates the FE-SEM micrographs of the fully sintered pellets of Gd^{3+} ion substitution BBTO Aurivillius ceramics from x = 0.00 to 0.30 respectively. The micrographs reveal a dense microstructure characterized by a random oriented plate-like grains. This is a general characteristic of Bismuth layered Aurivillius ceramics, which are reinforced plate-like grain formation layered structures [22]. The pronounced randomness of grain growth and the formation of thin, sharp plate—like grains are evident due to the anisotropic layered structure. Particularly, the growth rate along the a–b axis [22]. An interesting observation is the slight reduction in the thinness of the plate-like grains as the Gd concentration in BBTO ceramics increases. At higher dopant concentrations (x ≥ 0.10), exhibits a reduction in grain thickness. Hence, further dopant concentration of Gd^{3+} ions in BBTO host lattice may cause to even sharper thin plate like grains.

3.5 Temperature dependent dielectric spectroscopy

Dielectric spectroscopic studies were performed to observe the influence of Gd^{3+} ion-substitution on the diffuse relaxor-like behavior of the BBTO ceramics. Figure 6a–d illustrate the temperature-dependent relative dielectric permittivity (ε_r) of Gd^{3+} ion substitution BBTO Aurivillius ceramics in the temperature range 30–500 °C at selective frequency intervals (1 kHz to 1 MHz). The observed dielectric constant at RT is 160.65 at 1 MHz. With the increase of dopant concentration in BBTO ceramics, a slight increase in dielectric permittivity was noticed, i.e., 187.4, 195, and 217 for x = 0.10, 0.20, and 0.30 concentrations, respectively. A slight increase in dielectric constant was observed with the increase of temperature up to 250 ˚C, and above it, a sharp rise in dielectric constant was noticed for all Gd substituted BBTO samples [34, 35].

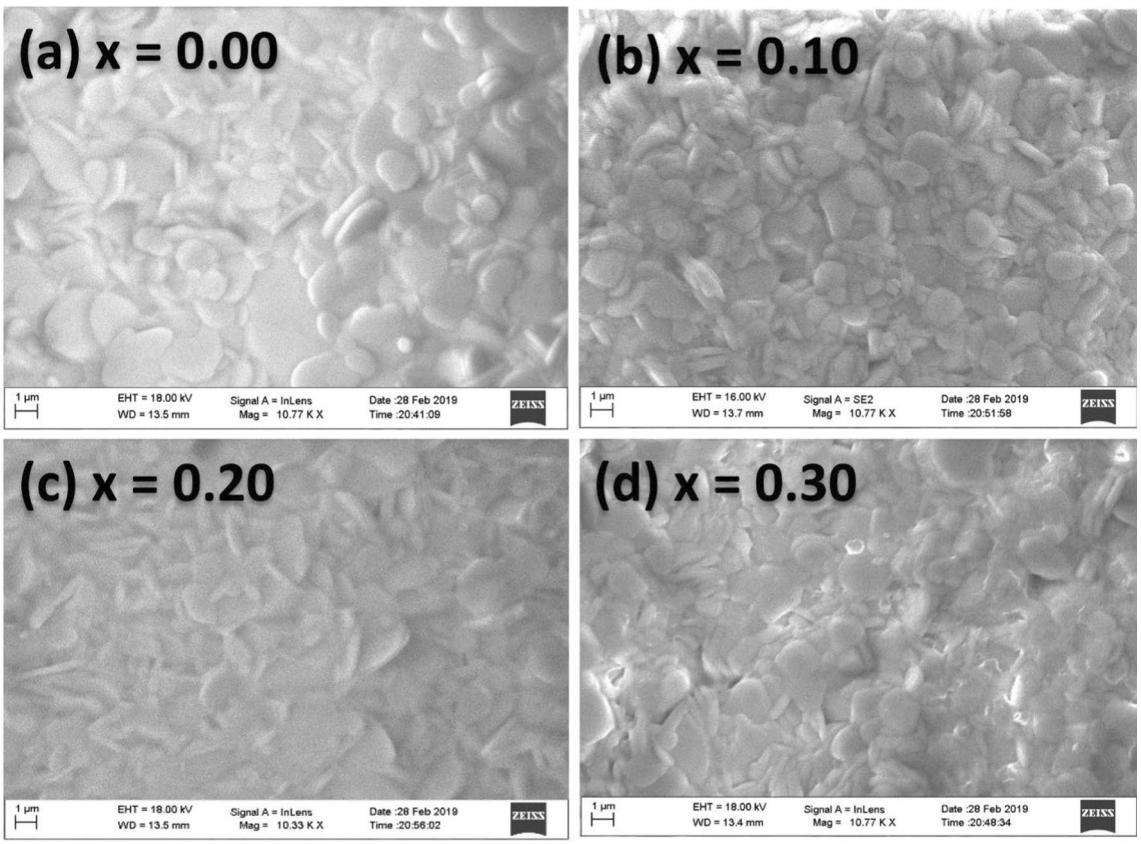

Fig. 5 **a–d** Typical FESEM images for a cross-sectional surface of $BaBi_{4-x}Gd_xTi_4O_{15}$ for dopant concentrations x = 0.00, 0.10, 0.20, and 0.30 ceramics respectively

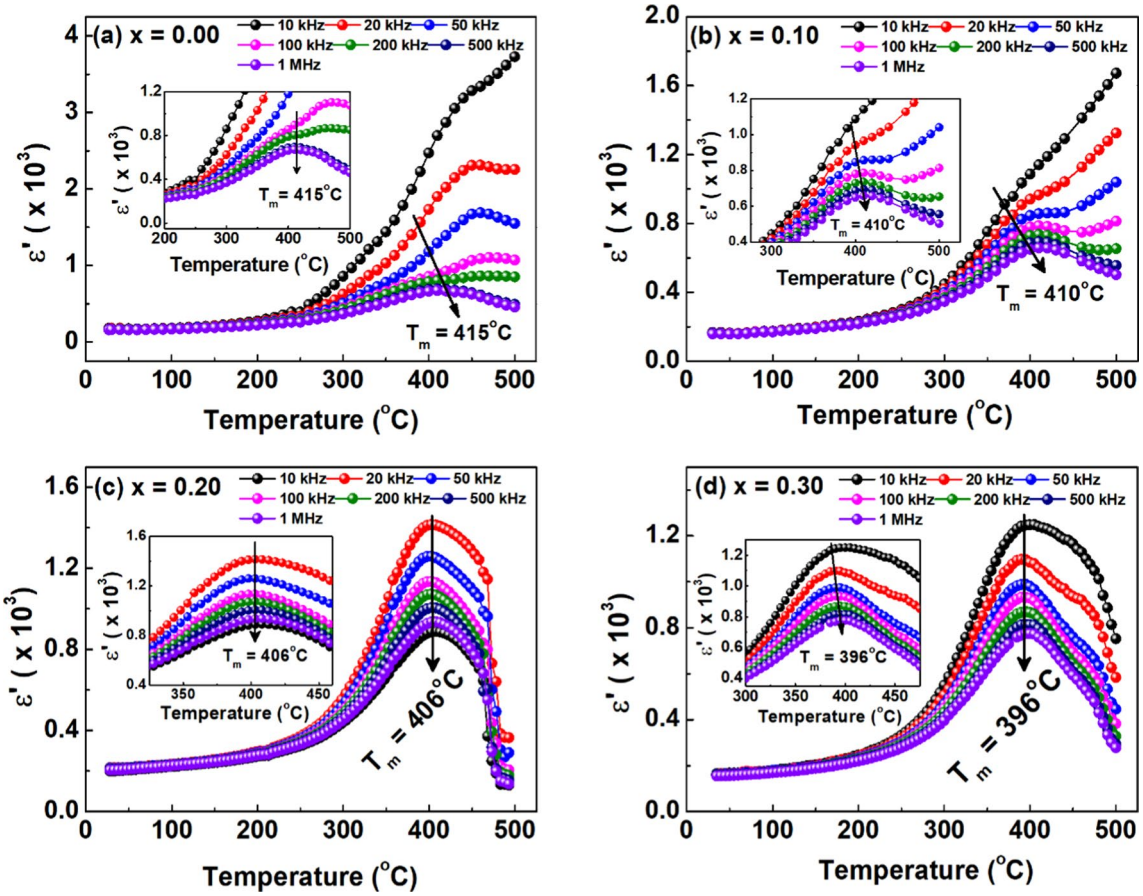

Fig. 6 **a–d** Variation of dielectric constant with temperature at selective frequency intervals from 10 to 1 MHz for $BaBi_{4-x}Gd_xTi_4O_{15}$ ceramics with dopant concentrations x = 0.00, 0.10, 0.20, and 0.30 respectively. Magnified view of dielectric constant near at Curie temperature region (shown in inset)

The temperature dependent dielectric constant with fixed frequency intervals is reported in Fig. 6a–d. For the pristine compound BBTO has degree of relaxation ($\Delta T_{relax} = T_{10\ kHz} — T_{100\ Hz}$) 18 ℃ and with increasing dopant Gd- in BBTO ceramics degree of relaxation decreases. For higher dopant above ≥ 0.20, reduced to minimum values 5 °C. therefore, it signifies a clear decreasing diffusivity with doped BBTO Aurivillius ceramics. It could be explained more clearly with correlation of temperature dependent spin-phonon mode analysis by temperature dependent Raman studies. T-dependent Raman spectroscopy reveals a conspicuous reduction in phonon mode frequencies as temperatures exceed 200 ℃, as depicted in Fig. 4a–c. Anomalies evident in the A_1 stretched vibration and A_2 mode of TiO_6 octahedra, exhibiting abrupt changes at temperatures nearing 200 ℃ and 250 ℃, specifically observed in highly Gd-doped ceramics. Furthermore, the Raman scattering analysis of temperature-induced Bi_2O_2 stretched modes corroborates these observations, especially as the dopant concentration escalates in BBTO ceramics. Notably, pristine, and lightly Gd-doped BBTO ceramics exhibit a decrement in wave number frequencies, except for values exceeding 0.20, as illustrated in Fig. 4a–c.

The incorporation of Gd^{3+} ions (from Gd_2O_3) as dopants confers robust thermal stability to the material, enabling it to endure high temperatures without compromising its crystalline integrity. Consequently, the presence of higher dopant concentrations facilitates stable mechanical stress and local atomic arrangement within the material, promoting inertial electric dipole moments. Hence, retain greater sustainability of long-range polar ordering in highly Gd-substituted BBTO ceramics. It was direct indicative of a transition from relaxor to normal ferroelectric behavior in high substituted BBTO ceramics [26].

Additionally, a slight frequency dispersion around the dielectric maximum (T_m) gradually shifts towards higher temperature regimes with increasing frequency noticed. This phenomenon serves as a characteristic signature of relaxor activity, accompanied by the observed decrease in dielectric maxima (ε_{max}) for all the measured samples [30]. This frequency dependent dielectric permittivity was termed as the diffuse relaxor activity. For BBTO ceramics,

the dielectric maximum observed at $T_m \sim 415$ ℃ at 1 MHz was attributed to the paraelectric-ferroelectric phase transition. This corresponds to a change in crystal structure from non-centrosymmetric orthorhombic-$A2_1am$ to centrosymmetric tetragonal-I4/mmm, as reported by Kumar and Varma 2009 et al. [36, 37]. Meanwhile, the observed dielectric maxima (TM) shift towards the high-temperature region with increasing frequency, along with the decrease in peak dielectric constant (ε_{max}). This indicates the persistence of diffuse or relaxor ferroelectric behavior in the pristine compound with a degree of relaxation behavior calculated with formula as $\Delta T_{relax} = T_{10\ kHz} — T_{1\ MHz} \simeq 18$ ℃

The variation of dielectric constant with temperature for fixed frequency intervals of Gd substituted BBTO ceramics is illustrated in Fig. 6b–d. As the concentration of Gd in BBTO increases, the dielectric maximum temperature termed the Curie Temperature (TM) shifts towards the lower temperature region for all Gd substituted BBTO ceramics. Decrease of Curie temperature towards lower temperature ascribes a more symmetric (paraelectric) phase transition in Gd- substituted BBTO ceramics.

The corresponding Curie temperatures (T_m) are 415 ℃, 410 ℃, 406 ℃, and 396 ℃ at a frequency of 1 MHz for x = 0.00, 0.10, 0.20, 0.30 ceramics respectively, and depicted in inset of Fig. 6a–d. A similar feature is found in the frequency and temperature-dependent dielectric plots, where the dielectric maximum (ε_{max}) decreases with increasing frequency as a function of temperature. Furthermore, the maximum dielectric constant (ε_{max}) value at T_C decreased with increasing Gd^{3+} ion concentration in BBTO ceramics. This behavior reflects the continuum diffusion/relaxor ferroelectric behavior even in Gd-substitution BBTO ceramics [38].

Temperature dependent dielectric loss (*tanδ*) peaks with selected frequency intervals of undoped and Gd-substituted BBTO ceramics were shown in Fig. 7a–d. The observed dielectric loss at RT of pristine compound BBTO is slightly

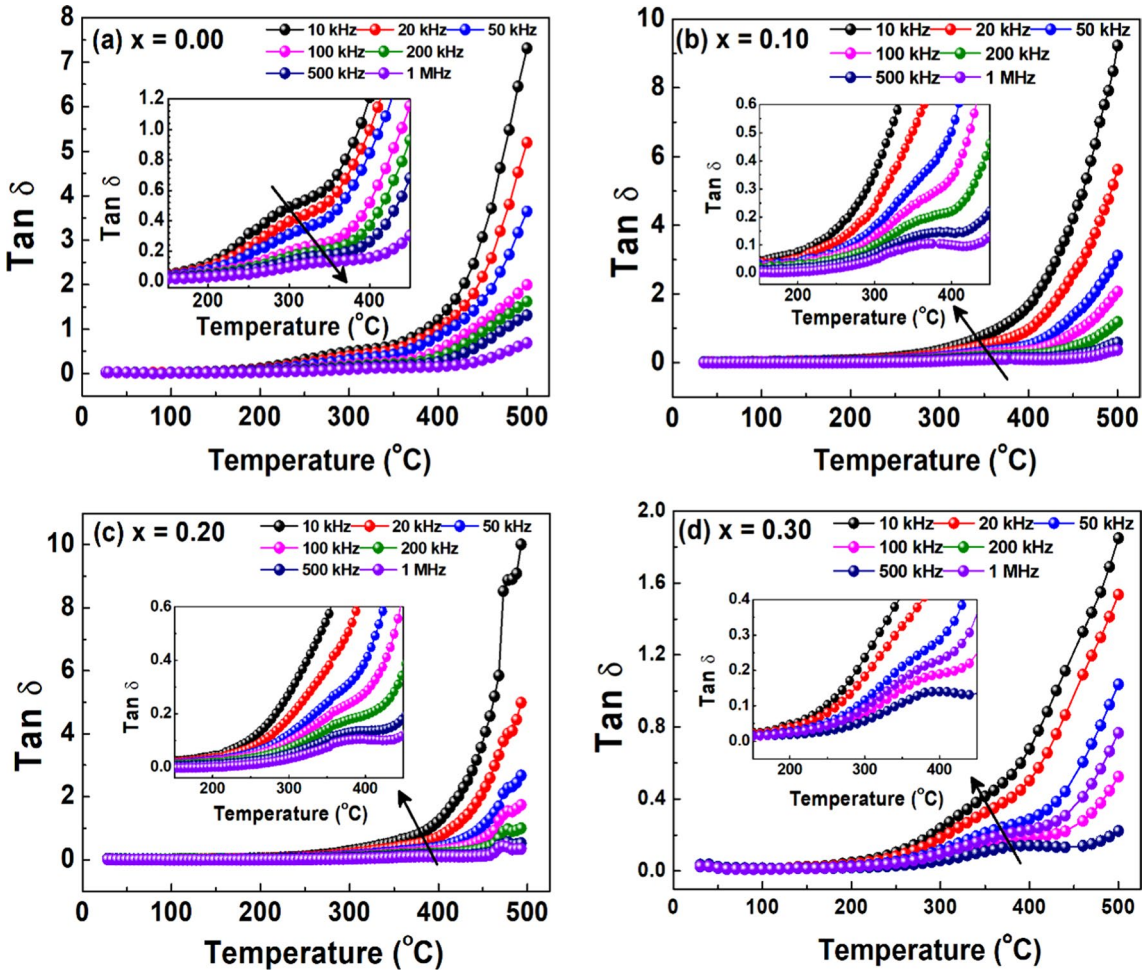

Fig. 7 **a–d** Variation of dielectric loss with temperature at selective frequency intervals from 10 to 1 MHz for $BaBi_{4-x}Gd_xTi_4O_{15}$ ceramics with dopant concentrations x = 0.00, 0.10, 0.20, and 0.30 respectively. Magnified view of dielectric loss near at Curie temperature region (shown in inset)

higher than that of Gd-substituted BBTO ceramics. With the increase of temperature, the observed dielectric loss peaks also exhibit the frequency-dependent behavior, which is slightly lower than T_m particularly in 350–390 ℃ intervals. Beyond T_m, a pronounced rise in the dielectric loss peak was noticed for all the Gd substituted BBTO Aurivillius ceramics. This might be due to an increased force in conductivity with temperature. These observations are well matched with recent reports on Ba-based Aurivillius ceramics [23, 38]. It is ascribed that at high sintering temperatures, the Bi-volatility might affect more in pure BBTO ceramics, pronouncing cationic vacancies as lattice defects. Henceforth, a large value of dielectric loss was noticed in pristine ceramics. With the introduction of dopant Gd in place of Bi ions, it leads to stabilizing the cationic defects and oxygen vacancies in the BO_6 octahedra of Gd substituted BBTO ceramics. As a result of this appropriate dopant substitution at Bi site, the effective reduction of dielectric loss was noticed.

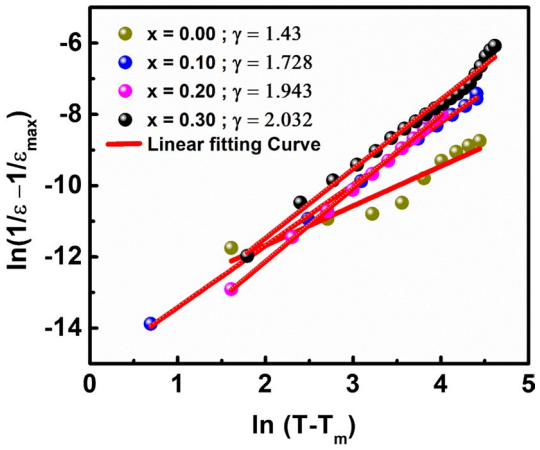

Fig. 8 Diffuse relaxor activity as shown in modified Curie law fitting curves: (**a**) Variation of ln $(\frac{1}{\varepsilon'} - \frac{1}{\varepsilon_{max}'})$ vs. ln $(T\text{-}T_m)$ @ 100 kHz frequency of $BaBi_{4-x}Gd_xTi_4O_{15}$ ceramics, (**b**) Variation of $(\varepsilon/\varepsilon_{max})$ vs. (T/T_{max}) for all measured samples

3.6 Origin of Relaxor property mechanism

Moreover, a noticeable diffuse relaxor activity is noticed with strong frequency dispersion near to Tm of dielectric peak ε_{max} (T), i.e., Tm shifts progressively towards higher temperature with increasing frequency for Gd-substituted BBTO ceramics. This is a signature of typical diffuse or relaxor ferroelectric nature stabilized in all the ceramic samples. The dielectric dispersion in the low frequency and high-temperature region indicates that the observed relaxor activity is not like pure relaxor in BBTO Aurivillius layered oxides. Indeed, the diffuse relaxor activity of $\varepsilon_{max}(T)$ in paraelectric region can be correlated to the Curie–Weiss law as well above the T_m. Below T_m, the deviation from the Curie–Weiss fitting is reported as proof of the development of the dipolar regions. To understand about the degree of diffuse length in the temperature range above ε_{max}, a modified form of the Curie–Weiss relation has been introduced as per the Eqns. 2, and 3. Worthwhile, a modified fitted curve between $\frac{\varepsilon_A(\omega)}{\varepsilon^1(T,\omega)}$ vs. $\frac{T}{T_m}$ was shown in Fig. 8 with increase of dopant concentration, a slight decrement in width was noticed [39–42]. It represents a clear modification in diffusivity and then crosses over to normal classical ferroelectric nature as emerged in highly Gd-substitution BBTO ceramics. To investigate the diffuse relaxor activity in all Gd-substituted BBTO samples, the modified Curie Weiss law can be enlightened by fitting dielectric plot for $ln(\frac{1}{\varepsilon'} - \frac{1}{\varepsilon_{max}'})$ vs. $ln(T - T_m)$ at 100 kHz as shown in Fig. 8 [23, 32, 43]. The slope of the curve represents the diffuseness constant (γ) as shown at the inset of Fig. 8a. The obtained γ values are drastically decreased with Gd concentration and then falls to γ =1.098 for x = 0.30 concentration. Other than the above, the Lorentz empirical relation $(\frac{\varepsilon_A(\omega)}{\varepsilon^1(T,\omega)}\ vs.\ \frac{T}{T_m})$ as shown in Fig. 8b also favors for the relaxor activity. Thus, this result clearly indicates a departure for both Curie–Weiss law as well as reported Lorentz empirical relation [2]:

$$\frac{1}{\varepsilon'} - \frac{1}{\varepsilon'_{max}} = \frac{(T - T_m)^{\gamma}}{C} (T > T_m) \tag{1}$$

$$\frac{\varepsilon_A(\omega)}{\varepsilon^1(T,\omega)} = \frac{\{1 + [(T - TA(\omega)]^2\}}{2\delta_A^2} \tag{2}$$

To generalize the inherent relaxor activity in ferroelectrics and the origin of diffuse relaxor behavior caused by random field polarizations is presence of polar nanoregions (PNRs) and polar nanodomains (PNDs) accounts for the relaxation mechanism. These two local structures introduce the nanoscale compositional heterogeneity, leading to modulated interfacial energies between polarizations and, thus, the dielectric relaxation mechanism [23, 43]. The local structure regarding creation of PNRs and PNDs was well explained in PMN perovskite systems by Cross and Viehland [44, 45]. For a perovskite unit cell, the relative displacement between cations and anions determines the overall polarization, resulting from the balanced local fields. Originating from the ferroelectric matrix, the polarization field plays the dominant role in local fields [46, 47]. In addition, the charge imbalance and mismatch atomic radii will lead to changes in local electric and strain fields. The origin of diffuse relaxor activity in dielectric characteristics are represented as degree of diffuseness and correlation length among the polar nano-regions. Interacting polar nano-regions should grow and enhance their correlation

length during cooling. Depending on the correlation length or the size of the polar regions, the sample may undergo (a) ferroelectric phase transition at T_m (for large correlation length) or (b) slowing down of polarization fluctuation at $T < T_m$ leading to random orientation of polar domains (for smaller correlation length) [48, 49]. To understand the inactive relaxor nature in Gd-substituted BBTO Aurivillius ceramics, the different relaxor models with fitting plots of ln*f* vs. 1000/T were adopted. Here, the frequency dispersions with the variation of T_m are fitted using four distinct relations i.e., (i) Arrhenius relation [Eq. (3)] (ii) Vogel-Fulcher relation [Eq. (4)] (iii) Cluster glass model [Eq. (5)] (iv) stretched string model [Eq. (6)] [49, 50]. The corresponding fitted graphs were shown in Fig. 9, 10, 11, 12 independent formula as given respectively.

$$f = f_o \exp\left(\frac{-E_a}{k_B T_m}\right) \tag{3}$$

$$f = f_o \exp\left(\frac{-E_a}{k_B (T_m - T_{VF})}\right) \tag{4}$$

$$f = f_o \left(\frac{T_m}{T_g} - 1\right)^{ZV} \tag{5}$$

$$f = f_o \exp\left(\frac{-E_a}{T_m}\right)^{P} \tag{6}$$

where f_o is the applied frequency ($2\pi f_o = \omega = 1/\tau$, τ is the microscopic time relaxation with flipping of fluctuating dipole entities), E_a is the activation energy, k_B is Boltzmann constant, T_{vf} is Vogel-Fulcher temperature related to the freezing of the polar cluster fluctuations, T_g is correlated with glass transition temperature, and *ZV* is the dynamic critical exponent, respectively [51–54].

The well-known Arrhenius (AR) equation [Eq. 3] is not appreciably fitted with the experimental data points, as shown in the Fig. 9. This indicates a lack of correlation with polar nano regions (PNRs) which are responsible for relaxor ferroelectricity. Additionally, the parameters (f_o and E_a) obtained from AR fit do not agree with the previous reports.

Furthermore, the Vogel-Fulcher (VF) equation [Eq. 4] presents an optimistic relation for the relaxor ferroelectrics, as depicted in Fig. 10. The frustrated interaction among the PNRs leads to freezing of the polar cluster fluctuations at a finite temperature (T_f). The parameters regarding VF fitting, such as relaxation time, activation energy, and *ZV* are well converged with earlier reports for relaxor ferroelectrics [55, 56]. The correlation regarding PNRs is further decreased with Gd-dopant in BBTO ceramics for concentrations x > 0.20. This results in a critical slowing down of the PNRs dynamics at higher Gd dopant concentrations. The

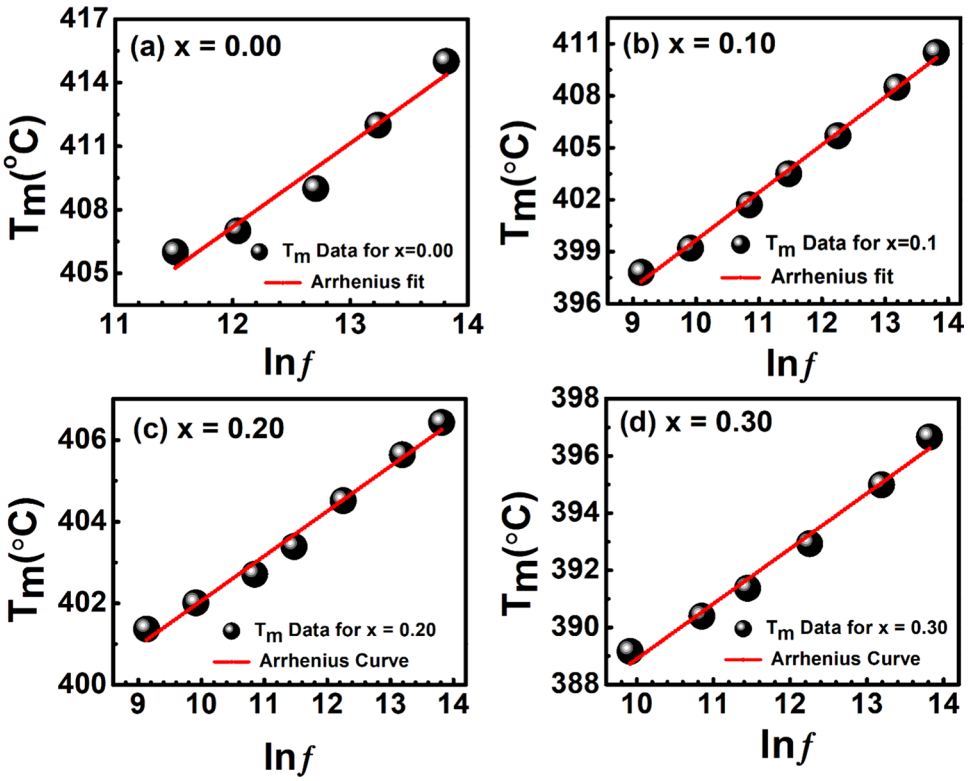

Fig.9 **a–d** Diffuse relaxor fitting curves based on Arrhenius (AR) relation for $BaBi_{4-x}Gd_xTi_4O_{15}$ ceramics from x = 0.00, 0.10, 0.20, and 0.30 respectively

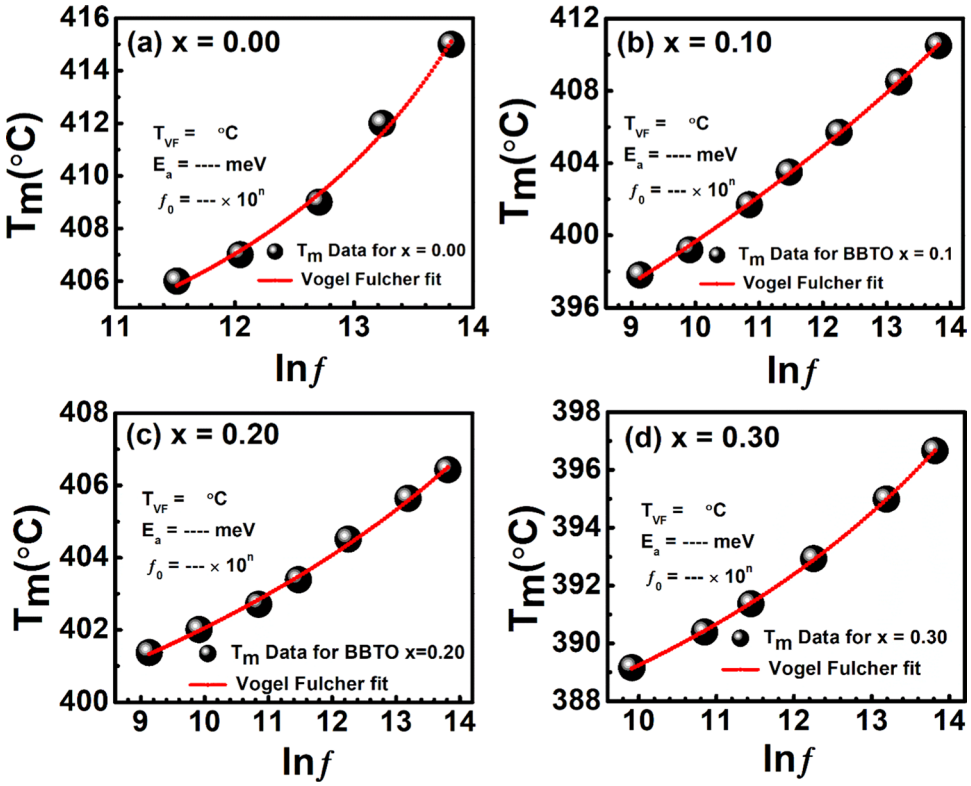

Fig.10 **a–d** Diffuse relaxor fitting curves based on Vogel-Fulcher (VF) relation for $BaBi_{4-x}Gd_xTi_4O_{15}$ ceramics from x = 0.00, 0.10, 0.20, and 0.30 respectively

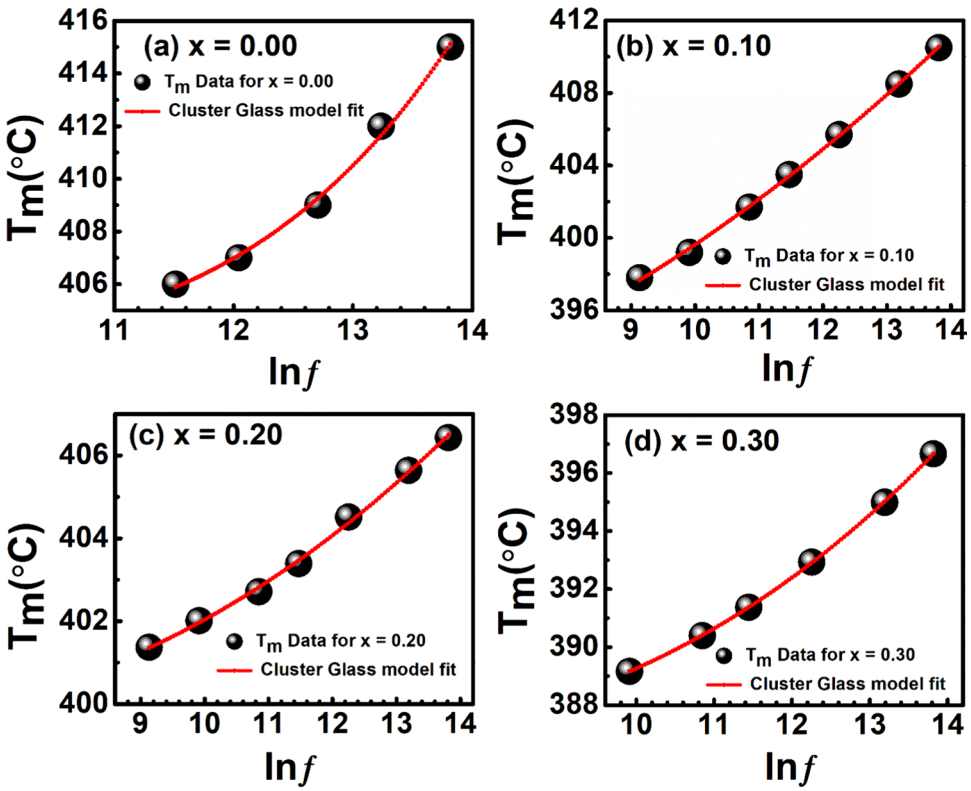

Fig.11 **a–d** Diffuse relaxor fitting curves based on Cluster Glass (CG) Model for $BaBi_{4-x}Gd_xTi_4O_{15}$ ceramics from x = 0.00, 0.10, 0.20, and 0.30 respectively

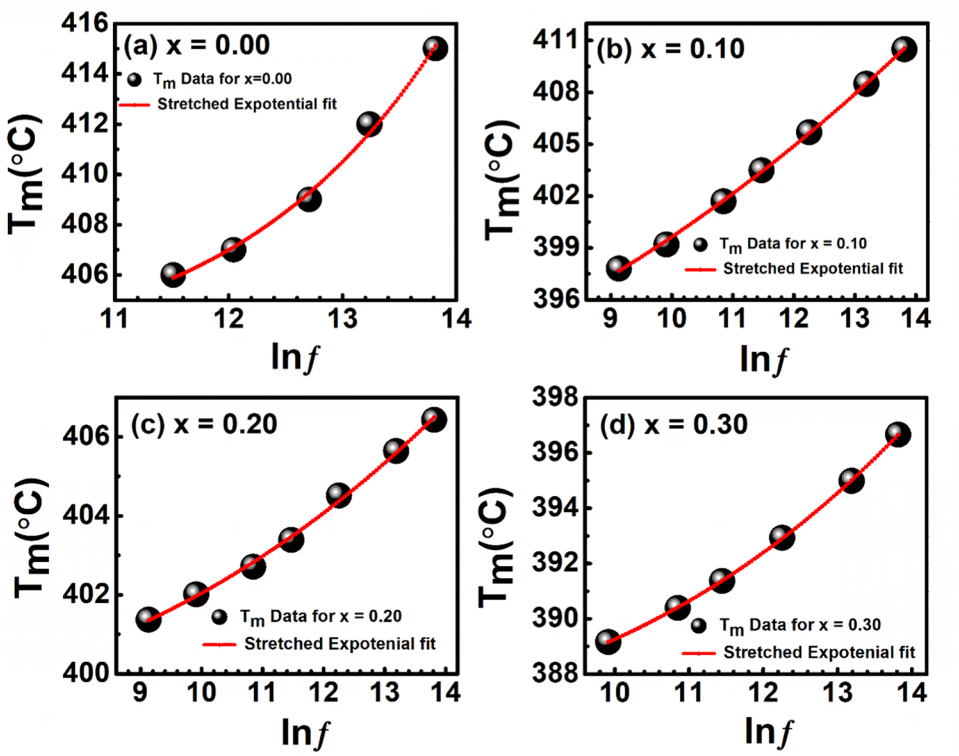

Fig.12 **a–d** Diffuse relaxor fitting curves based on stretched string (SS) model for $BaBi_{4-x}Gd_xTi_4O_{15}$ ceramics from x = 0.00, 0.10, 0.20, and 0.30 respectively

obtained activation energy and relaxation time are attributed to positional disorder of cations in A or B sites of perovskite blocks, interrupting the evolution of long-range polar ordering could lead to sustainability in highly Gd-substituted BBTO Aurivillius ceramics, deviating from relaxor to classic ferroelectric character. Thus, this observation directly represents the diffusion of VF relaxor activity in Gd-substituted BBTO Aurivillius ceramics [46, 55–57].

Figure 11a–d includes the comparative fitting ($T_m vsf$) to the cluster glass (CG) relation [Eq. 5] for x = 0.00 to 0.30 concentration. Worthwhile, the reasonable fitting parameters of cluster glass temperatures (T_{GS}) and *ZV* i.e., critical dynamic exponent for the correlation length were correlated to the frustrated interaction among the PNRs resulting in a critical slowing down of PNR's dynamics near T_{GS} temperature. In other words, the obtained relaxation frequency (f_o) for all fitted equations regarding different concentrations is prominent and deviates from reasonable relaxation frequencies for critical slowing down of PNR's dynamics. Hence, the calculated values from cluster glass relation also violate cluster glass-like behavior in Gd-substituted BBTO Aurivillius ceramics at higher concentrations. Moreover, the stretched string (SS) exponential relationship [Eq. 6] is fitted and depicted in Fig. 12a–d, where interaction between the polar clusters is considered to slow down the polar cluster dynamics. The freezing of polar cluster dynamics takes place only at 0 K. The obtained 'p' represented the degree of relaxation and f_o are not well-considered in comparison with the relaxation strength of relaxor for normal ferroelectrics. Thus, the corresponding fitted input parameters for Arrhenius (AR), Vogel Fulcher (VF), cluster glass (CG) and stretched string (SS) models for all Gd substituted BBTO ceramics ($0.00 \leq x \leq 0.30$) are presented in Table 2. Therefore, we can conclude the attempt made regarding diffuse relaxor, the fit parameters calculated from the AR, CG, and SS model are not unrealistic for any thermally activated process in Gd substituted BBTO ceramics [47, 49, 58]. The significantly good fit has been obtained from VF and CG models and are agreed with the relaxation frequencies with PNR domains for pristine compound. For higher dopant concentration (x > 0.20) in Gd doped BBTO ceramics, VF model is an appropriate fit.

3.7 Ferroelectric polarization studies

Polarization (P)_vs Electric field (E) hysteresis is the direct characterization technique to understand the ferroelectric nature. Figure 13 illustrates the room temperature P—E hysteresis loops for Gd-modified BBTO ceramics under the applied maximum electric field (E_{max}) of 50 kV/cm at loop frequency of 1 Hz. The undoped BBTO exhibits well saturated polarization loop at a E_{max} of 50 kV/cm, where the saturation polarization (P_s) is 2.45 μC/cm^2, the remnant polarization (P_r) is 1.45 μC/cm^2, and the coercive field E_c is 2.45 kV/cm, respectively. Therefore, the undoped BBTO compound, with its large areal loss energy density indicates

Table 2 Relaxor ferroelectric activity parameters and corresponding activation energies, etc. using Arrhenius, Vogel-Fulcher, Cluster Glass, and Stretched String models for Gd substituted BBTO ceramics from x = 0.00 to 0.30 mol%

Model → Composition ↓	Arrhenius (AR)	Vogel—Fulcher (VF)	Cluster—Glass (CG)	Stretched string (SS)
x = 0.00		T_{VF} = 394.11 ℃	T_{SG} = 403.50 ℃	P = − 7.89
	f_0 = 51.93536683	$f_0 = 18.8118 \times 10^6$	$f_0 = 1.9248 \times 10^2$	$f_0 = 23.3885 \times 10^3$
	E_a = 0.030 eV	$E_a = 525.12 \times 10^{-5}$ eV = 5.25 meV	Z_v = 5.05	E_a = 0.034 eV
x = 0.10		T_{VF} = 392.42 ℃	T_{SG} = 389.64 ℃	P = − 2.05
	f_0 = 15.18032224	$f_0 = 4.0706 \times 10^{14}$	$f_0 = 9.299 \times 10^2$	$f_0 = 20.491291 \times 10^3$
	E_a = 0.032 eV	E_a = 0.117 meV	Z_v = 1.83	E_a = 0.034 eV
x = 0.20		T_{VF} = 388.43 ℃	T_{SG} = 399.63 ℃	P = —2.73
	f_0 = 2.974274073	$f_0 = 1.2356 \times 10^{11}$	$f_0 = 4.9402 \times 10^2$	$f_0 = 6.9228 \times 10^2$
	E_a = 0.031 eV	E_a = 0.183 meV	Z_v = 2.1	E_a = 0.0342 eV
x = 0.30		T_{VF} = 374.39 ℃	T_{SG} = 386.8 ℃	P = − 3.54
	f_0 = 6.889510242	$f_0 = 2.0683 \times 10^9$	$f_0 = 5.68263 \times 10^2$	$f_0 = 11.414 \times 10^3$
	E_a = 0.0317 eV	E_a = 0.147 meV	Z_v = 2.66	E_a = 0.0314 eV

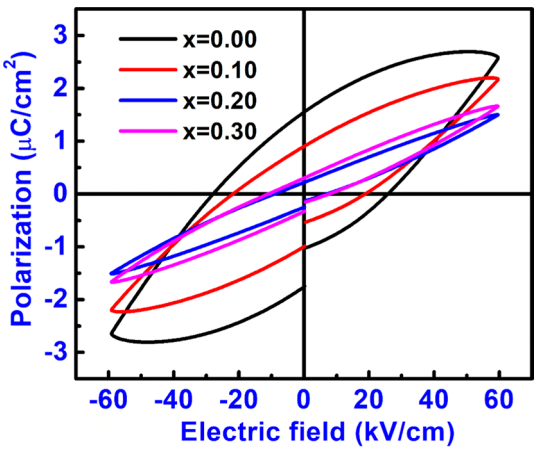

Fig. 13 **a–d** Room temperature P-E loops for $BaBi_{4-x}Gd_xTi_4O_{15}$ ceramics with dopant concentrations x = 0.00, 0.10, 0.20, and 0.30 respectively

a hard-ferroelectric polarization nature. On the other hand, the Gd-substituted BBTO ceramics exhibit a soft ferroelectric nature having with low loss energy density [47, 49, 58]. With increasing Gd-concentration in BBTO, the observed P_s decreases remarkably from 2.45 to 0.54 μC/cm^2, while the coercive field (E_c) is drastically reduced from 2.12 to 0.5 kV/cm. Consequently, owing to the effect of domain wall turning, the Gd—substituted BBTO ceramics lead to a more predominant movement from diffuse relaxor to soft ferroelectric character. These results are consistent with the outcomes of diffuse dielectric studies using different models for relaxors.

4 Conclusion

The Gd^{3+} ion substituted BBTO Aurivillius ceramics was synthesized successfully by conventional solid-state reaction method. The Rietveld refined XRD pattern confirmed the dopant of higher concentration is more stable for orthorhombic crystal system with dual symmetry ($A2_1am + F2mm$) space group. Furthermore, the Raman spectroscopic analysis supported the microstructural modification caused for existence of dual phase at higher Gd concentration. Surface morphology and elemental analysis confirms the homogeneous presence in elemental purity and plate like grains with non-uniform randomness of Aurivillius ceramics phase. Temperature dependent dielectric studies confirmed a shifting of Curie temperature (T_m) towards low temperature region with the increase of concentrations of Gd dopant in BBTO ceramics. Observed diffuse relaxor ferroelectric property explained with suitable models, indicated well stable relaxor only for low concentration of dopant (Gd; $x \leq 0.10$) BBTO ceramics, and crossover relaxor to ferroelectric for high concentration ($x \geq 0.20$) because of intrinsic suppressed interaction of polar regions. A slim and thin unsaturated ferroelectric P-E loop confirmed a soft and weak relaxor ferroelectric character in Gd-substitution BBTO ceramics.

Acknowledgements The work was supported by Researchers Supporting Project number (RSPD2024R765), King Saud University, Riyadh, Saudi Arabia.

Authors contributions TP conceptualized and contributed to the analysis and draft writing. KSKRCS and DSS conducted T – dependent dielectric studies. AG was involved in data acquisition and formal analysis. AMT and PR contributed to formal analysis, editing, and reviewing the manuscript.

Data availability The data that support the findings of this study are available from the corresponding author upon reasonable request."

Declarations

Conflict of interest The authors declare that there is no conflict of interest.

References

1. J. Portelles, N.S. Almodovar, J. Fuentes, O. Raymond, J. Heiras, J.M. Siqueiros, J. Appl. Phys. **104**, 73511 (2008)
2. A.A. Bokov, Z.-G. Ye, J. Mater. Sci. **41**, 31 (2006)
3. J. Carreaud, P. Gemeiner, J.-M. Kiat, B. Dkhil, C. Bogicevic, T. Rojac, B. Malic, Phys. Rev. B **72**, 174115 (2005)
4. C.A.-P. de Araujo, J.D. Cuchiaro, L.D. McMillan, M.C. Scott, J.F. Scott, Nature **374**, 627 (1995)
5. B. Aurivillius, Ark. Kemi **1**, 463 (1949)
6. E.C. Subbarao, J. Phys. Chem. Solids **23**, 665 (1962)
7. T. Jardiel, A.C. Caballero, M. Villegas, J. Ceram. Soc. Japan **116**, 511 (2008)
8. J. F. Scott, Berlin (2000).
9. A. Ando, T. Sawada, H. Ogawa, M. Kimura, Y. Sakabe, Jpn. J. Appl. Phys. **41**, 7057 (2002)
10. B.H. Park, B.S. Kang, S.D. Bu, T.W. Noh, J. Lee, W. Jo, Nature **401**, 682 (1999)
11. B.J. Kennedy, Q. Zhou, Y. Kubota, K. Kato, J. Solid State Chem. **181**, 1377 (2008)
12. P. Nayak, K. Mitra, S. Panigrahi, Mater. Lett. **216**, 54 (2018)
13. J. Tellier, P. Boullay, M. Manier, D. Mercurio, J. Solid State Chem. **177**, 1829 (2004)
14. S.K. Rout, E. Sinha, A. Hussian, J.S. Lee, C.W. Ahn, I.W. Kim, S.-I. Woo, J. Appl. Phys. **105**, 24105 (2009)
15. P. Fang, H. Fan, Z. Xi, W. Chen, Solid State Commun. **152**, 979 (2012)
16. J.D. Bobić, M.M.V. Petrović, N.I. Ilić, E. Palaimiene, R. Grigalaitis, C.O. Paiva-Santos, M. Cilence, B.D. Stojanović, Ceram. Int. **41**, 309 (2015)
17. I. Pribošič, D. Makovec, M. Drofenik, J. Eur. Ceram. Soc. **21**, 1327 (2001)
18. A. Khokhar, P.K. Goyal, O.P. Thakur, A.K. Shukla, K. Sreenivas, Mater. Chem. Phys. **152**, 13 (2015)
19. J. Chen, Z. Tang, B. Yang, S. Zhao, Appl. Phys. Lett. **113**, 153904 (2018)
20. P. Nayak, T. Badapanda, S. Panigrahi, Mater. Lett. **204**, 120 (2017)
21. F. Rehman, L. Wang, H.-B. Jin, P. Ahmad, Y. Zhao, J.-B. Li, J. Alloys Compd. **709**, 686 (2017)
22. M. Reddyprakash, S.K. Rout, A. Satapathy, T.P. Sinha, S.M. Sariful, Ceram. Int. **42**, 8798 (2016)
23. J.D. Bobić, M.M.V. Petrović, J. Banys, B.D. Stojanović, Ceram. Int. **39**, 8049 (2013)
24. T. Patri, A. Ghosh, M.L.V. Mahesh, P.D. Babu, S.K. Mandal, M.N. Singh, Sci. Rep. **12**, 16508 (2022)
25. P. Fang, H. Fan, J. Li, L. Chen, F. Liang, J. Alloys Compd. **497**, 416 (2010)
26. K.C. Sekhar, T. Patri, A.M. Tighezza, D.S. Saini, P. Rosaiah, A. Ghosh, Appl. Phys. A **130**, 150 (2024)
27. S. Kumar, K.B.R. Varma, J. Phys. D Appl. Phys. **42**, 75405 (2009)
28. Z. Li, M. Yang, J.-S. Park, S.-H. Wei, J.J. Berry, K. Zhu, Chem. Mater. **28**, 284 (2016)
29. Y. Chen, J. Xu, S. Xie, Z. Tan, R. Nie, Z. Guan, Q. Wang, J. Zhu, Materials (Basel). **11**, 821 (2018)
30. Ming-Wen Chu, Maria-Teresa Caldes, Luc Brohan, Marcel Ganne, Marie, Olivier Joubert, and Yves Piffard "Bulk and Surface Structures of the Aurivillius Phases: Bi4-xLaxTi3O12 ($0 \leq x \leq 2.00$)" Chem. Mater. 16, 1, 31–42, (2004)
31. S. Ivantchev, E. Kroumova, G. Madariaga, J.M. Perez-Mato, M.I. Aroyo, J. Appl. Crystallogr. **33**, 1190 (2000)
32. C.H. Hervoches, A. Snedden, R. Riggs, S.H. Kilcoyne, P. Manuel, P. Lightfoot, J. Solid State Chem. **164**, 280 (2002)
33. M. Osada, M. Tada, M. Kakihana, T. Watanabe, H. Funakubo, Jpn. J. Appl. Phys. **40**, 5572 (2001)
34. T. Badapanda, R.K. Harichandan, A. Mishra, S. Anwar, J. Adv. Dielectr. **3**, 1350013 (2013)
35. B.J. Kennedy, Y. Kubota, B.A. Hunter, K. Kato, Solid State Commun. **126**, 653 (2003)
36. D.Y. Suárez, I.M. Reaney, W.E. Lee, J. Mater. Res. **16**, 3139 (2001)
37. S.M. Pilgrim, A.E. Sutherland, S.R. Winzer, J. Am. Ceram. Soc. **73**, 3122 (1990)
38. A. Khokhar, M.L.V. Mahesh, A.R. James, P.K. Goyal, K. Sreenivas, J. Alloys Compd. **581**, 150 (2013)
39. V. Koval, I. Skorvanek, G. Viola, M. Zhang, C. Jia, H. Yan, J. Phys. Chem. C **122**, 15733 (2018)
40. Y.L. Du, G. Chen, M.S. Zhang, Solid State Commun. **131**, 313 (2004)
41. J. Zhu, X. Chen, Z. Zhang, J. Shen, Acta Mater. **53**, 3155 (2005)
42. M.P. Moret, R. Zallen, R.E. Newnham, P.C. Joshi, S.B. Desu, Phys. Rev. B **57**, 5715 (1998)
43. J.D. Bobić, R.M. Katiliute, M. Ivanov, N.I. Ilić, A.S. Dzunuzović, M.M.V. Petrović, J. Banys, B.D. Stojanović, J. Alloys Compd. **702**, 619 (2017)
44. L.E. Cross, Ferroelectrics **151**, 305 (1994)
45. D. Viehland, S.J. Jang, L.E. Cross, M. Wuttig, Phys. Rev. B **46**, 8003 (1992)
46. Z. Cheng, L. Zhang, X. Yao, J. Appl. Phys. **79**, 8615 (1996)
47. W. Kleemann, J. Dec, Phys. Rev. B **94**, 174203 (2016)
48. N. Bontemps, J. Rajchenbach, R.V. Chamberlin, R. Orbach, Phys. Rev. B **30**, 6514 (1984)
49. W. Kleemann, S. Miga, Z.K. Xu, S.G. Lu, J. Dec, Appl. Phys. Lett. **104**, 182910 (2014)
50. W. Kleemann, J. Adv. Dielectr. **2**, 1241001 (2012)
51. A.A. Bokov, Y.-H. Bing, W. Chen, Z.-G. Ye, S.A. Bogatina, I.P. Raevski, S.I. Raevskaya, E.V. Sahkar, Phys. Rev. B **68**, 52102 (2003)
52. A.R.P. Rau, W. Zhao, Phys. Rev. A **68**, 52102 (2003)
53. D. Viehland, S.J. Jang, L.E. Cross, M. Wuttig, J. Appl. Phys. **68**, 2916 (1990)
54. D. Viehland, J.F. Li, S.J. Jang, L.E. Cross, M. Wuttig, Phys. Rev. B **43**, 8316 (1991)
55. Z.-Y. Cheng, R.S. Katiyar, X. Yao, A. Guo, Phys. Rev. B **55**, 8165 (1997)
56. J. Souletie, J.L. Tholence, Phys. Rev. B **32**, 516 (1985)
57. W. Kleemann, S. Miga, J. Dec, J. Zhai, Appl. Phys. Lett. **102**, 232907 (2013)
58. W. Kleemann, J. Dec, S. Miga, Phase Transitions **88**, 234 (2015)